JOURNAL OF AIRCRAFT
Vol. 47, No. 3, May–June 2010

Influence of Wing Configurations on Aerodynamic Characteristics of Wings in Ground Effect

Juhee Lee,* Chang-suk Han,† and Chang-Hwan Bae‡
Hoseo University, Asan Chungnam 336-795, Republic of Korea

DOI: 10.2514/1.46703

A numerical analysis is performed to investigate the aerodynamic characteristics and the static height stability of the endplate and the anhedral angle on an aspect-ratio-one wing-in-ground effect. The analysis shows that the ground effect increases the lift by the high pressure on the lower surface, reduces the drag, increases the suction on the upper surface, and considerably enhances the lift–drag ratio. The endplate, which prevents the high-pressure air from escaping out of the lower surface and reduces the influence of the wing-tip vortex, further augments the lift and the lift–drag ratio. Irodov's criteria are also numerically evaluated in order to investigate the static height stability. The comparison of Irodov's criteria shows that the endplate is not favorable for the static height stability. However, the anhedral angle improves the lift as well as Irodov's criteria at various angles of attack and heights. Interestingly, the stagnation point for the anhedral angle moves forward with decreasing height at the low angles of attack and leads an increase in the pressure drag at the leading edge. This increase nullifies the advantages of the induced drag and the pressure drag. Thus, the lift–drag ratio of a wing is not improved as much with an anhedral angle as it is with an endplate.

Nomenclature

AR	=	aspect ratio
b	=	span, m
C_D	=	drag coefficient
C_d	=	sectional drag coefficient
C_L	=	lift coefficient
C_l	=	sectional lift coefficient
C_M	=	pitching moment
C_p	=	pressure coefficient
c	=	chord
HS	=	static height stability in Eq. (7)
h/c	=	nondimensional height at trailing edge
k	=	turbulent kinetic energy
L/D	=	lift–drag ratio
Re	=	Reynolds number
v_∞	=	free stream velocity, m/s
$y^+_{\max}$	=	maximum value of shear Reynolds number on the wing surface
α	=	angle of attack, deg
ε	=	dissipation of turbulent kinetic energy
ω	=	vorticity
ω_n	=	nondimensional vorticity, $\omega/(v_\infty/c)$

I. Introduction

ACCORDING to the globalization and information technology of industries, transportation has become a central factor in key industries over the last decade. The von Karman–Gabriell diagram [1] depicts the efficiency of various transportations. A remarkable thing in the diagram is the triangular area at the center of the technology line, in which no conventional means of transportation appears. The wing-in-ground (WIG) effect craft, a flying ship cruising with the speed of 100 to 400 km/h and with lift–drag ratios of 15 to 30, can fill the speed and efficiency gap between the marine and air transports seen in the diagram. In general, the lift and drag forces of a wing will change considerably near the ground. These phenomena during the takeoff and landing have been observed by many researchers [2–5] from as early as the 1900s. According to their results, the ground has a great influence (suction and stagnation) on the pressure distributions along the wing surface. Oncoming air to the lower wing surface gradually decreases the magnitude of the speed and changes to static pressure. This eventual increase of pressure is called an air cushion or a ram effect.

Wieselsberger [2] performed a theoretical investigation to determine the conditions in taking off and landing of an airplane using Prandtl's wing theory. He used the principle of reflection and replaced the surface of the ground by a second wing at the same distance but on the opposite side. The reduction in the induced drag of a monoplane and a multiplane in-ground effect (IGE) was estimated in terms of the ground clearance, the aspect ratio, and the lift coefficient. The theoretical predictions agree well with the experimental results. Wieselsberger noted that a longer runway for a landing was necessary because of an excessive lift due to this air cushion. The pressure distributions on the lower surface became somewhat constant, and the strength of the pressure increased with the ground proximity caused by the air cushion. On the other hand, the pressure distribution on the upper surface varied with the suction and the wing profile.

In general, the pressure rise on the lower surface is considerably high when the wing is IGE, and the resultant forces of the pressure lead to an increase in lift. On the contrary, the center of the pitching moment tends to move to the midchord, where it is behind the center of gravity. The stability of the wings IGE is also changed according to the center of the pitching moment. For finite wings IGE, the induced drag is decreased because of the decreased influence of the wing-tip vortex, whereas the strength of the wing-tip vortex is increased. Joh and Kim [6] compared the total pressures of the vortex core for IGE ($h/c = 0.3$) and out-of-ground effect (OGE) cases, and they found that the vortex strength grew with the ground proximity, whereas the induced drag was reduced.

Ahmed et al. [5] and Hsiun and Chen [7] predicted the flow characteristics of the NACA 4412 by experimental and numerical methods. A sudden increase in the lift coefficient was observed as the ground was approaching, because a stationary wall boundary for the

Received 11 August 2009; revision received 30 November 2009; accepted for publication 1 December 2009.

*Lecturer, Mechatronic Engineering, 165 Sechul-ri. Member AIAA.
†Professor, Department of Defense Science and Technology, 165 Sechul-ri.
‡Lecturer, Mechatronic Engineering, 165 Sechul-ri.

ground was used. This increase did not happen in a real flight. Both investigations found an increase in the suction on the upper surface and an increase in the pressure on the lower surface in the two-dimensional flow. For $\alpha = 0$, the lift was almost zero at $h/c = 0.05$ due to the strong suction effect on the lower surface and the laminar separation. The endplate prevents the flow from exiting through the wing-tip instead of the small gap at the trailing edge and ultimately increases the ground effect exerted on the wing surface.

Recently developed WIG effect vehicles are generally equipped with an endplate and/or an anhedral angle to improve their aerodynamic performance and stability. However, the aerodynamic characteristics on the endplate have not been fully investigated in both experimental and/or numerical research until now. Only a few experimental investigations on the effect of an endplate were performed by Fink and Lastinger [3] and Carter [4]. Fink and Lastinger [3] performed a series of wind-tunnel investigations to determine the ground effect on the aerodynamic characteristics of thick and highly cambered wings with various aspect ratios. They used the two wings on opposite sides of the imaginary ground. All the wings in the experiments increased the lift slope and reduced the induced drag, which resulted in an increase of the lift–drag ratio. Because of the constant pressure distributions on the lower surface, they predicted an increase in the height stability at positive angles of attack but a decrease at negative ones. They also observed a reduction in the induced drag without a change in the wing profiles as the wing approached the ground. The effect of the endplate, which was extended below the wing, and its height were identical with that of the trailing edge, as briefly mentioned in the study. According to their investigation, an endplate showed the effect of preventing the stagnated air on the lower surface from flowing out around the wing tips and produced a substantial improvement in the lift–drag ratio. On the other hand, the ground had no effect on the maximum lift of the plain wings but reduced the maximum lift coefficient of the wings equipped with split or slotted flaps [8].

Recently, Park and Lee [9] carried out a numerical investigation into the effect of an endplate at various angles of attack and ground clearances. They found that the endplate prevented the high-pressure air from escaping out of the lower wing surface, reduced the influence of the wing-tip vortex, and augmented the lift and lift–drag ratio further. The endplate also reduced the deviation of the static height stability with respect to the pitch angles and heights. However, the comparison of Irodov's stability criteria showed that the endplate was not favorable for static height stability.

Many numerical and experimental studies have been performed to predict the aerodynamic characteristics of wings IGE. However, much less study has been devoted to analyzing the flow field around an endplate and an anhedral angle. From the aerodynamic point of view, the influence of the endplate and the anhedral angle to the aerodynamic characteristics and the stability is significant. Therefore, in the present work, the influence of the endplate and the anhedral angle on the aerodynamic characteristics of a rectangular WIG effect is studied numerically. Numerical analyses are performed by solving the Reynolds averaged Navier–Stokes (RANS) of turbulent flow, and the aerodynamic characteristics are compared for the case of a plain wing, a wing with an endplate, and a wing with an anhedral angle for various conditions, such as the angles of attack and the nondimensional heights.

II. Computational Models and Validation

The physical configuration of the endplate considered in this study is presented in Fig. 1. Air is taken, as the fluid and the flow of the air is assumed to be steady, incompressible, and turbulent. The shape of the endplate is three dimensional. The fluid properties are taken to be constant, and the effect of the viscous dissipation is assumed to be negligibly small. Using the aforementioned assumptions, the RANS equations for mass and momentum, which are written in a tensor notation, have to be solved:

$$\frac{\partial(\rho u_j)}{\partial x_j} = 0 \tag{1}$$

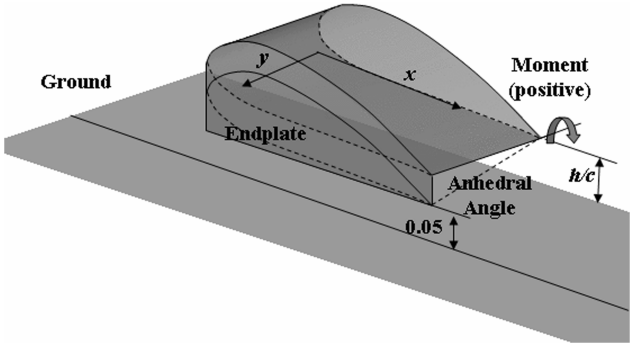

Fig. 1 Geometrical definition of h/c and pitching moment and coordinate system.

$$\frac{\partial(\rho u_i u_j)}{\partial x_j} = -\frac{\partial P}{\partial x_i} + \frac{\partial}{\partial x_j}\left[\mu\left(\frac{\partial u_i}{\partial x_j} + \frac{\partial u_j}{\partial u_i}\right) - \overline{\rho u_i' u_j'}\right] \tag{2}$$

The last term, $\overline{\rho u_i' u_j'}$ (the Reynolds stress), must be modeled by using a turbulence model in order to solve the RANS equations. In this study, the flow domain was divided into two regions, such as the near-wall and the fully turbulent regions, and then adopted a standard turbulent model [10] and wall function next to the wall. According to this model, k and ε are expressed in a tensor form as follows:

$$\frac{\partial}{\partial x_j}(\rho u_i k) = \frac{\partial}{\partial x_j}\left[\frac{\mu_t}{\sigma_k}\frac{\partial k}{\partial x_j}\right] + P_k - \rho\varepsilon \tag{3}$$

$$\varepsilon = \frac{k^{3/2}}{l_\varepsilon}\left(1 + \frac{C_\varepsilon}{Re_y}\right) \tag{4}$$

where $i = 1, 2$, and 3 denotes x, y, and z directions, respectively. The term P_k in Eq. (3) stands for the production term. The model constants and various functions used in the turbulent model are detailed in [10].

The numerical simulations presented in this work were done by means of STAR-CD [11], which is a general purpose commercial software. The pressure–velocity coupling phenomenon is resolved through the SIMPLE algorithm [12]. For representing the exact flight conditions, the moving wall boundary condition with a flight velocity is applied at the ground. The solutions are treated as converged ones when the sum of the normalized residual is less than 1×10^{-7}.

The numerical results for the modified Glenn Martin 21 airfoil IGE, $h/c = 0.167$, are obtained by the present method and compared with the experimental data in [3]. The three consecutive numbers of meshes (about 130,000; 250,000; and 380,000) are used for the validation and the mesh dependency test of the computational model. The computations are performed at $\alpha = 0$, with $AR = 1$ and $Re = 0.46 \times 10^6$. The endplates are not attached in these validation cases. The modified Glenn Martin 21 airfoil is listed in Table 1, and the bottom of the wing is flat from 30% of the chord to the trailing edge. Figure 2 depicts the comparisons of C_L and the drag polar at $h/c = 0.167$ and shows a good agreement with the experiments. The renormalization group k–ε model is used for predicting the turbulent flow, and the near-wall flow is computed by using a wall function. Because of the geometric symmetry of the wing, only half of the model is simulated. Five layers of the prism mesh are used to resolve the boundary layer on the wing surface, and the $y^+_{\max}$ values are about 50 over the wing surface. For the precise results, the refined mesh (about 380,000 cells) is used in this study. The boundary conditions were configured to identify the free-flight condition. The upstream boundary was modeled using a velocity inlet boundary condition with a uniform velocity distribution. The downstream boundary was modeled using a pressure outlet boundary condition. The symmetric boundary condition at the center of the wing span, $y/c = 0$, is applied. A slip wall boundary condition was imposed on the undisturbed far boundary, therefore imposing a zero crossflow condition. The wing and ground plane were modeled as solid walls with a

Table 1 Modified airfoil section of Glenn Martin 21 [3]

	Airfoil ordinates	
x/c	Upper	Lower
0.000	0.0886	0.0860
0.0125	0.1221	0.0603
0.025	0.1381	0.0479
0.050	0.1598	0.0333
0.075	0.1765	0.0235
0.100	0.1892	0.0172
0.150	0.2072	0.0075
0.200	0.2168	0.0028
0.300	0.2213	0
0.400	0.2113	0
0.500	0.1920	0
0.600	0.1664	0
0.700	0.1335	0
0.800	0.0943	0
0.900	0.0500	0
0.950	0.0257	0
1.000	0	0

no-slip boundary condition enforced. In addition, the ground surface was provided with a velocity equal to freestream for identifying free flight through the calm air. The details of the comparison between this study and the experiment can be found in the previous study by Park et al. [13].

III. Results and Discussion

A computational analysis of a finite wing is performed with the same grids and numerical schemes as discussed in the preceding section. The computational domain used in this study is extended 10 times of a chord for each direction to avoid the influence of the far boundaries, but it is extended 30 times for the downstream direction. To take the wake behind the wing into account correctly, dense grids are used in an extended area of four times of a chord. The grid system and the computational domain are shown in Fig. 3. The nondimensional height between the wing and the ground is measured at the trailing edge, and the nose-up pitching moment is positive, as shown in Fig. 1. In Fig. 1, the downward endplate is placed at the wing tip, and the bottom edge of the endplate is parallel to the ground surface. The distance between the endplate and the ground remains constant, irrespective of the height and angle of attack, in order to predict the aerodynamic performance for the cruise condition. The definition of an anhedral angle in this study is a constant height between the ground and the wing tip, as shown in Fig. 1. The numerical calculation with the endplate and the anhedral angle is restricted from $h/c = 0.1$ to 0.3 because of their constant gap to the ground ($0.05c$). When $h/c \geq 0.5$, the length of the endplate is unreasonably long.

A. Drag and Lift Coefficients

To explain the effect of the endplate and the anhedral angle on the lift according to h/c, C_L for the various values of $\alpha = 0 \sim 10$ deg are displayed in Figs. 4 and 5. Figures 4 and 5 show the results of three different wing configurations: a plain wing, a wing with an endplate, and one with an anhedral angle. As shown in Figs. 4 and 5, they agree well with the general ground effect that the proximity to the ground results in an increase of C_L except with $\alpha = 0$ deg. In general, the lift of the WIG effect depends on three facts: the suction on the upper wing surface, the divergent–convergent passage on the lower wing surface, and the pressure augmentation on the lower surface by the stagnation of the oncoming air. Only the divergent–convergent passage or the thickness effect is not favorable for the augmentation of the lift. For instance, a symmetric airfoil without a camber or an airfoil with a moderate camber recorded lower values of

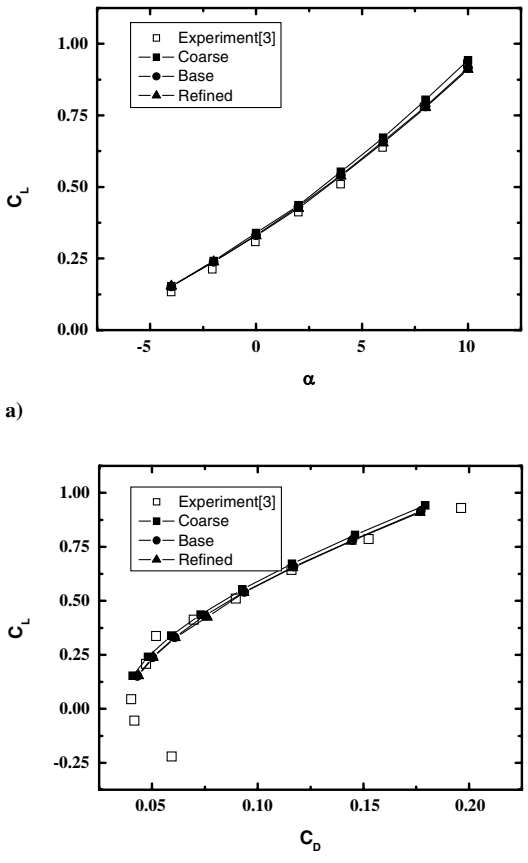

Fig. 2 Validation and mesh dependency test of computational model: a) lift coefficient at $h/c = 0.167$ and b) drag polar at $h/c = 0.167$.

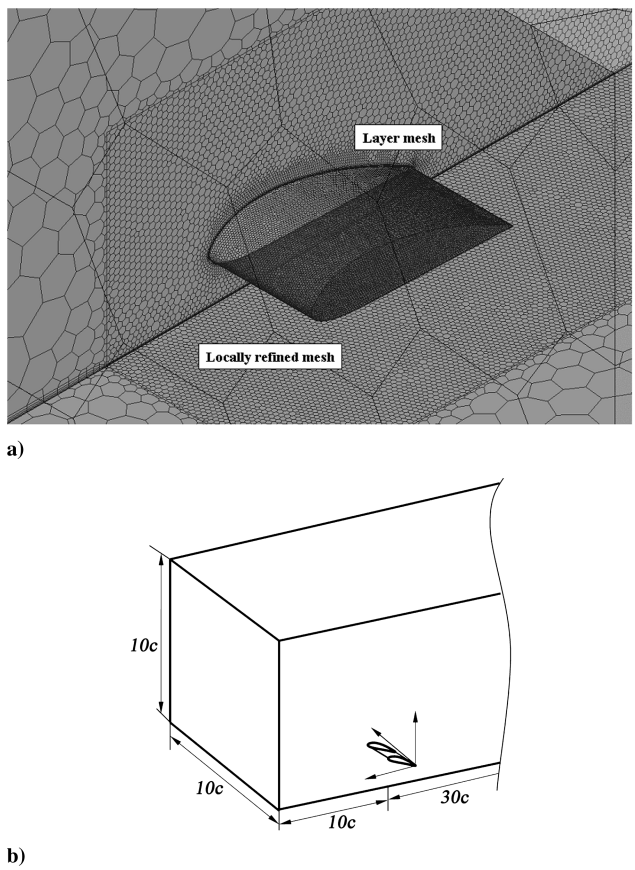

Fig. 3 Grid systems and computational domain: a) polyhedral meshes and prism layers on the wing and ground and b) computational domain and wing.

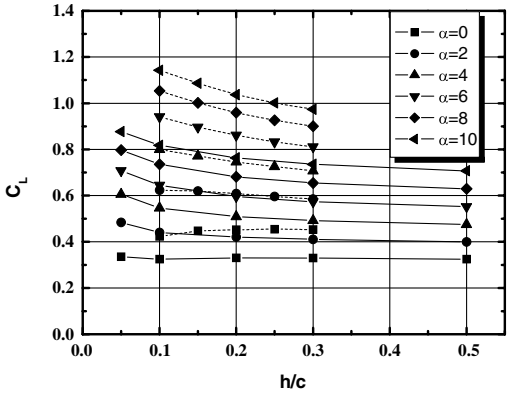

a)

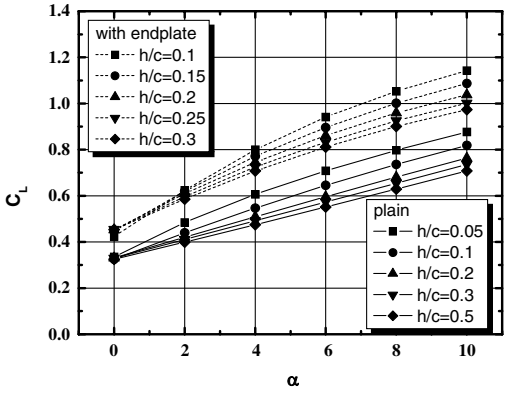

b)

Fig. 4 C_L of plain wing: a) C_L with respect to h/c and b) C_L with respect to α (dotted line for wing with endplate and solid line for plain wing).

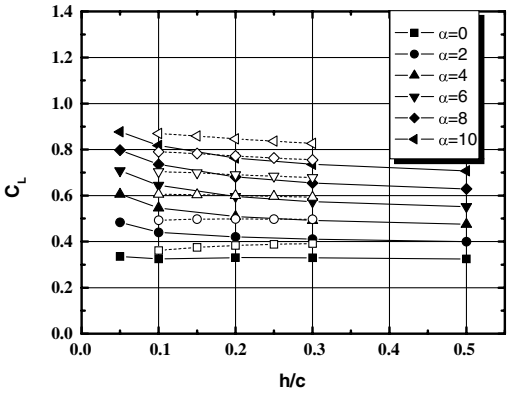

a)

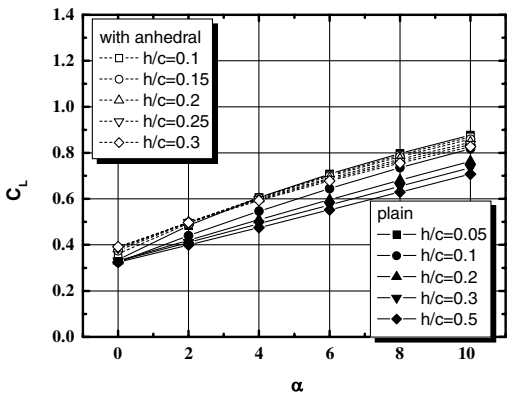

b)

Fig. 5 C_L of wing with endplate: a) C_L with respect to h/c and b) C_L with respect to α (dotted line for wing with anhedral angle and solid line for plain wing).

the lift with ground proximity because of its divergent–convergent passage or thickness effect, as reported in [6,7]. Ahmed and Sharma [14] showed different results in their experiment with a symmetric airfoil of a NACA 0015. The difference is caused by both the blockage effect and the nonslip ground plate.

A modified Glenn Martin 21 airfoil for the WIG effect vehicle used in this study has a geometrical advantage and somewhat reduces the deep decrease of the lift by the thickness effect (divergent–convergent passage) at low angles of attack. The same results can be found in the study by Ahmed and Goonaratne [15]. Their study on the same wing profile, different low-aspect ratios, and a different endplate shape showed that the wing could provide a lift augmentation when they were under the influence of ground effect. In Fig. 4a for the plain wing, the values of the lift slightly increase at $\alpha = 2 \sim 8$ deg as the wing approaches the ground. These increases in lift at the lower height tend to the wing back to the original height when the wing decreases the height. It is possible to say that the Glenn Martin 21 wing profile without an endplate and an anhedral angle is, therefore, stable in height at positive angles of attack. On the other hand, it can be seen in Fig. 4 that the existence of an endplate captures the increase of the lift when compared with the case of a plain wing for all conditions because of the higher pressure under the wing, that will be shown later. That is, the endplate brings on an increase in the lift at the same α and h/c. However, the values of lift forces in Fig. 4a are virtually decreased with the reduced height at $\alpha = 0$ deg. The decrease in lift at low α, which is observed in some research [3,5,6], is caused by the thickness effect, which will be discussed later. However, for the case of the wing with an anhedral angle, some of the wing tip will be continuously influenced by ground effect, because the height at the wing tip is held constant, irrespective of its h/c. Because of the wing tip IGE, the increase of the lift with lower height is linear, but the deviation of that is small, as shown in Fig. 5a. Thus, it can be said that the ground effect of the wing with an anhedral angle reaches higher than that of the plain wing. For the wing with an anhedral angle, constant lift coefficients with height can be clearly seen at $\alpha = 2$ deg and, on the other hand, decrease of lift with the decreased height can be observed at $\alpha = 0$ deg, whereas the only one-point decrease of C_L at the same angle of attack is recorded for the case of the endplate. These lift drops mainly come from an increase in suction and a decrease in ram effect on the lower wing surface. The ram effect (the stagnation of the oncoming air on the lower wing surface) is dominant at $\alpha > 4$, and C_L gradually increases with a decreasing height. It is interesting that, in Fig. 4b, C_L is increased with α suddenly when the wing is sufficiently close to the ground (such as $h/c \leq 0.1$), whereas the increment for all heights ($0.1 \leq h/c \leq 0.3$) can be observed in Fig. 5b. The fact that the influence of the ground effect with the endplate and with the anhedral angle reaches higher than the plain wing can be deduced from Figs. 4b and 5b.

The drag coefficients for various values of α and h/c are shown in Fig. 6. In general, the wings at $h/c \geq 0.5$ are completely OGE and, thus, the significant changes of drag may not be observed. However, for $h/c \leq 0.3$, because the wings begin to be affected by the ground effect, the drag coefficients change nonlinearly for all three cases. The drag force can be decomposed nominally into its pressure drag, induced drag, and friction drag. The skin friction, which is proportional to the wetted area of a wing surface, is almost constant with respect to the height, but it is slightly variable with respect to α. Consequently, the contribution of the skin friction to the total drag is not significant. The total drags on the wing are varied with the balance of the induced drag and the pressure drag, with respect to the heights and angles of attack, as shown in Fig. 6. When the wing is sufficiently close to the ground and at low angles of attack, the effect of the pressure drag to the total drag, except around the leading edge, is relatively small because of its normal direction perpendicular to the flow stream. A constant drag with respect to height is recorded at $\alpha = 8$ deg for the plain wing in Fig. 6a, at $\alpha = 4$ for the wing with an endplate in Fig. 6a, and at $\alpha = 2$ for the wing with an anhedral angle

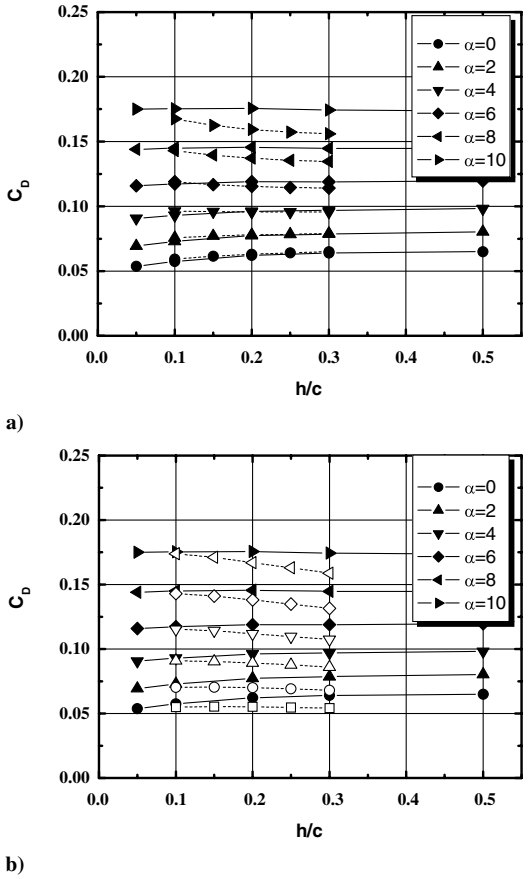

Fig. 6 C_D with respect to h/c: a) plain wing and wing with endplate and b) plain wing and wing without anhedral angle (solid line and filled shape for plain wing, dotted line and filled shape for endplate, and dotted line and hollowed shape for anhedral angle).

in Fig. 6b. Increases in drag can be seen after these constant-drag lines, with reducing h/c in Fig. 6. Even though the results cannot be compared directly because of the different definition of height, which was defined as a quarter chord, Fink and Lastinger [3] also observed the constant drag at $\alpha = 6$ deg. Ahmed and Goonaratne [15] performed the experiment and noted that the drag coefficient remains constant with increasing ground clearance for a particular flap angle. Ahmed and Sharma [14] observed that the drag coefficient increased slightly with the ground clearance. In the two-dimensional analysis [7], the drag also decreased with the decreasing height because of the change of the pressure drag of the airfoil IGE. The theoretical treatment of ground effect presented by Wieselsberger [2] showed the reduction of the induced drag for a wing with the decreased height. In general, the induced drag and the friction drag decrease with the reduction of the height, whereas the pressure drag may vary with the angle of attack and the wing profile while the pressure on the lower wing surface increases. For a low angle of attack, the pressure, except around the leading edge, does not considerably contribute to the increase in drag because of the normal direction of the wing surface. However, it is quite interesting to realize that the drag for the wing with an anhedral angle increases with the decreasing height, but for the plain wing and the wing with an endplate, it decreases. One decisive factor in the increased drag is the location of the stagnation point, where the normal direction of the leading edge is parallel to the flow stream. Ahmed et al. [5] also noted that the location of the stagnation point was one of the significant factors for the increase in drag, but they did not show the effect in the experiment. For the case of an anhedral angle, a contribution of the stagnation pressure at the leading edge is significant to the total drag. Owing to the computational method, the force on the local wing surface can be plotted in each direction: the x and y directions. The summation of the x direction and the y direction will be the drag and the lift, respectively. As a result, the contribution of each force on the local area to the total drag can be visualized. To investigate the changes of the pressure drag on the leading edge, the x-direction forces on the wing surface with $\alpha = 6$ deg are plotted in Fig. 7. Quantitatively, the total drag coefficient increases from 0.794 to 0.852 with the reduction of the height from $h/c = 0.3$ to 0.1, whereas the contribution of the friction drag decreases from 0.113 to 0.105. Even though it is impossible to

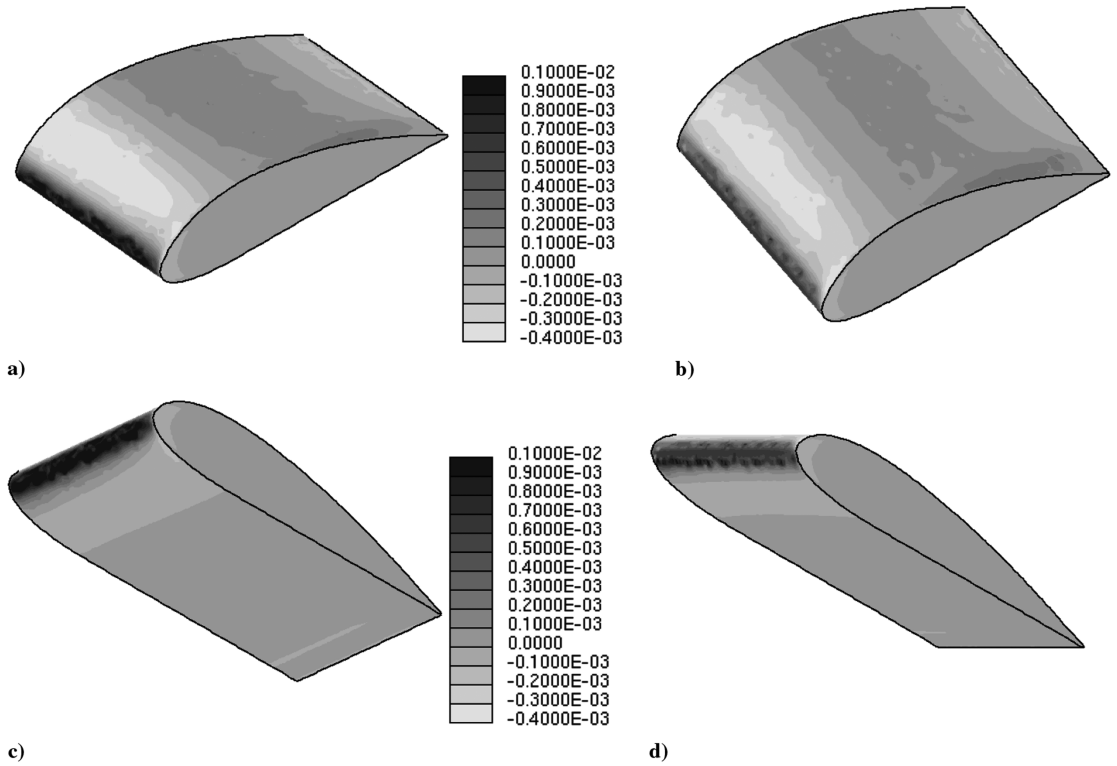

Fig. 7 Drag (x-direction force) of wing with anhedral angle at $\alpha = 0$: a) upper surface at $h/c = 0.1$, b) upper surface angle at $h/c = 0.3$, c) lower surface at $h/c = 0.1$, and d) lower surface at $h/c = 0.3$.

separate the induced drag from the total drag, the induced drag also decreases with the reduction of the height. As a result, only the pressure drag is increasing. As shown in Fig. 7, the contribution of the lower wing surface to the drag is not significant because of its normal direction of the wing surface. The only differences are shown around the leading edge. This drag force on the leading edge cancels the drag reductions, the induced drag, and the friction drag with decreasing height at a low angle of attack. It may be concluded that the contribution of the stagnation on the leading edge to the drag coefficient is significant in a low angle of attack when the wing approaches the ground.

Figure 8 depicts the lift–drag ratios (L/D). It can be clearly seen that the wing with an endplate has a larger value of the lift–drag ratios than those of the other two cases. The lift–drag ratios for the plain wing in Fig. 8a exponentially increase with decreasing height, whereas those for the wing with an endplate linearly increase and those for the wing with an anhedral angle in Fig. 8b decrease. The maximum lift–drag ratios for the case with the endplate are recorded at $\alpha = 4$ deg, whereas those for the plain wing and the wing with an anhedral angle are at $\alpha = 2$ deg. The endplate improves L/D due to an increase in the lift by the air cushion on the lower wing surface and a decrease in the induced drag. Steep decreases of L/D with an endplate are observed at $\alpha = 0$ deg by a decrease in the lift because of the thickness effect, as shown in Fig. 4a. In a different case, L/D for the anhedral angle decreases with the lower height. This decrease mainly comes from a decrease in lift at the low angles of attack and an increase in drag at high angles of attack, as shown in Figs. 5 and 6. Raymond [16] carried out experiments for the three different airfoils (Martin No. 2, R.A.F 15 special, and U.S.A. 27) and showed that L/D with respect to height was lessened at a high α.

The aerodynamic characteristics of lift and drag can be wrapped in a single diagram: the drag polar. Virtually improving the aerodynamic performance of wings IGE can be achieved by an increase in lift as well as a reduction of the drag at the same time. Thus, a high-performance airfoil may be placed at the left-top corner in a drag polar. In Fig. 9, the drag polar shows that the rapid increase in drag for the case of the plain wing and the wing with an anhedral angle is observed with an increase in lift. However, the increase in drag for the endplate is not as significant as found in the others. The drag for the wing with an endplate is much lower and is expected to have a higher aerodynamic performance. As a result, it can be deduced that the wing with an endplate may have a stronger acceleration capability, a higher aerodynamic performance, and a longer operation range. On the other hand, comparing the drag polars for the plain wings with different heights, $h/c = 0.5$ (square) and $h/c = 0.1$ (circle), clearly shows that the ground effect improves the lift–drag ratio with a lower height by increasing the lift and reducing the drag. This agrees well with the general ground effect. Further improvement can be observed for the wing with anhedral angle (see the reverse triangles in Fig. 9).

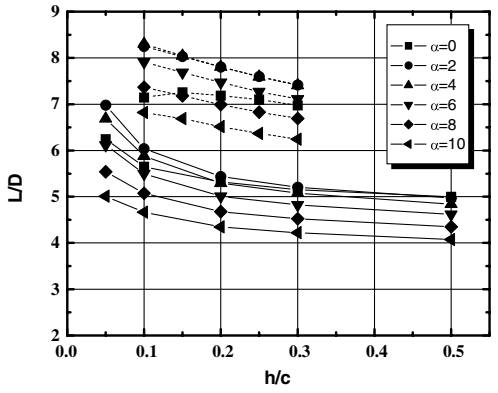

a)

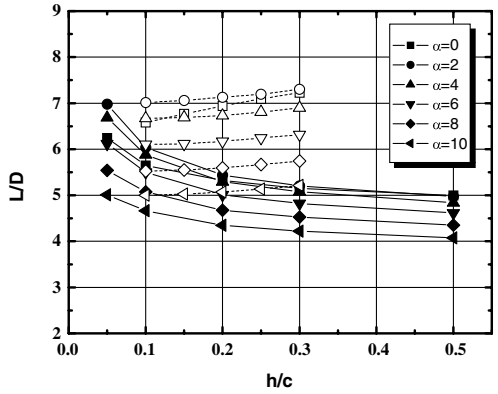

b)

Fig. 8 L/D with respect to h/c: a) plain wing and wing with endplate and b) plain wing and wing with anhedral angle (solid line and filled shape for plain wing, dotted line and filled shape for endplate, and dotted line and hollowed shape for anhedral angle).

B. Static Height Stabilities

The aerodynamic forces of wings IGE, which are affected by changes in α as well as h/c, lead to a different stable condition from OGE or an airplane. The HS condition for the WIG effect that considers both α and h/c was proposed by Irodov [17] and is plotted in Fig. 10. Irodov derived with a coordinate system that has its origin at a trailing edge. In this study, the same coordinate system was used for convenience. The calculation of HS includes the differentiations of C_L and C_M against h/c and α. To avoid numerical errors and excessive calculations, the differentiations are evaluated from the interpolation functions of C_L and C_M instead of the direct numerical differentiations. Although an interpolation function is used, the proper differentiation value at $\alpha = 0$ cannot be obtained because of the sudden increase of numerical errors by the small values in a denominator. Therefore, the comparison of HS at $\alpha = 0$ deg is ruled out in Fig. 10. Two different functions, a second-order polynomial for the lift coefficient and double exponential functions [6] for C_M, are employed:

$$C_L = C_{L0} + A_1\alpha + A_2\alpha^2 \tag{5}$$

$$C_M = C_{M0} + B_1 e^{h/c/t_1} + B_2 e^{h/c/t_2} \tag{6}$$

where C_{L0}, A_1, A_2, C_{M0}, B_1, t_1, B_2, and t_2 are independent variables for the curve regression. Finding independent variables for C_L and C_M can be an optimization problem to find a curve minimizing the deviation between the curve and the points of C_L and C_M. In this study, the genetic algorithm [18] (global optimization technique) is used to find the proper interpolation curves:

$$HS = \frac{C_{M,\alpha}}{C_{L,\alpha}} - \frac{C_{M,h}}{C_{L,h}} = X_\alpha - X_h \le 0 \tag{7}$$

where h and α represent the derivative of the height and the angle of attack, respectively. C_M are measured at a trailing edge. One might expect that the simplest condition for the static height stability is

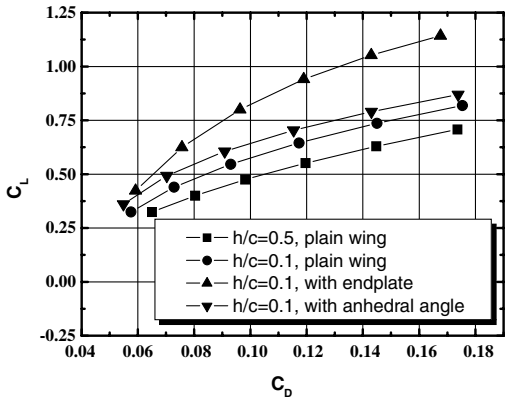

Fig. 9 Drag polars.

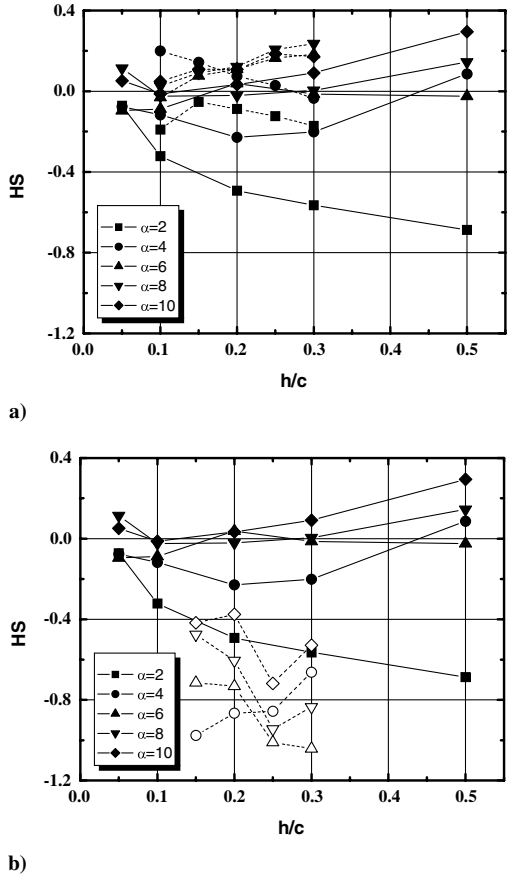

Fig. 10 *HS* with respect to h/c: a) plain wing and wing with endplate and b) plain wing and wing with anhedral angle.

$$C_{L,h} < 0 \tag{8}$$

When the increase of the height will indeed lead to the decrease of the lift, it apparently satisfies the stable condition of height. The fact that C_M changes due to the height is not, however, taken into account in Eq. (8). Therefore, the equation is only valid when the wing is in a trimmed condition; in other words, C_M must be held constant. Equation (7) takes into consideration the actual conditions: C_M and C_L according to α and h/c. As shown in Eq. (7), HS implies the distance between two neutral points: X_h for the neutral point of heights and X_α for the neutral point of angles. The positive direction of x, a distance measured from the trailing edge, is upstream. Consequently, the HS condition can be satisfied if X_h is upstream of X_α. Figures 10a and 10b apparently show decreases of HS, with respect to h/c, at $\alpha = 2$ and 4 deg and increases at $\alpha = 6 \sim 10$ deg. These changes mainly come from X_h. Changes of the X_α against heights and angles of attack, which are not plotted, are moderate and linearly decrease as the height decreases. This implies that C_L and C_M are linearly increased as α and the rate is not changed much, except the ground is extremely close to the ground. The HS condition for the case with the endplate is only satisfied at $\alpha = 2$ deg.

Different from the other cases, all the points of HS for the wing with an anhedral angle in Fig. 10b satisfy the condition of the static height stability. It can be deduced that an anhedral angle is favorable for HS. On the other hand, HS is increasing, except $\alpha = 4$ deg as the height decreases. X_α is closer to the tailing edge than the other cases, but X_h goes further upstream. As a result, the case with an anhedral angle can satisfy the HS condition and has a sufficient stability margin. This improvement of HS may promote using an anhedral angle in WIG effect vehicles: especially, a Lippisch-type wing (a reverse delta wing with an anhedral angle) is generally used for the small-sized ones. There is a practical condition for the static height stability in [19]; the center of gravity should be located between X_h and X_α. A wing without an endplate, for which X_h is placed near to the quarter chord, is more favorable for X_h.

C. Surface Pressure Distributions

In Figs. 11 and 12, the pressure distributions on the wing surface show the effect of the endplate and the anhedral angle in detail. For the cases of ground effect, a considerable increase and decrease in pressure are found on the lower surface and the upper surface, respectively. The air, which tends to stagnate under the airfoil due to the ground effect, causes a reduction in velocity and an increase in pressure on the lower surface. The suction on the upper surface increases slightly due to the divergence of the flow toward the upper surface. Moreover, the endplate prevents the flow from exiting through the wing tip instead of the small clearance at the trailing edge and, consequently, helps to augment the lift further. A higher pressure on the lower surface by the stagnation of the oncoming air is also observed in the studies on a NACA 4412 [5,7] but a lower pressure on the upper surface is not. A modified Glenn Martin 21 airfoil, used in this study, has a divergence of the flow toward the upper surface and improves the lift further. In Fig. 11b, the circular symbols show the significantly high pressures on the lower surface at the wing tip, which have the same magnitude as that at the midspan in Fig. 11a. It is deduced that the endplate, which prevents air from exiting at a wing tip, keeps a high pressure on the lower surface until it reaches the wing tip. The wiggles on the upper surface imply the existence of the wing-tip vortex at that point. The augmentation of the flow stagnation on the lower wing surface and the increase of the suction on the upper wing surface are the main reasons of an increase of C_L IGE. Because the high-pressure flow under the wing surface rapidly escapes from the wing tip on a plain wing, the wing does not keep its high pressure, and a pressure loss in the area grows rapidly. For the wing with an anhedral angle, in Fig. 11, the pressure by the air cushion on the lower surface increases, but the suction on the upper surface decreases. Therefore, the advantage of an air cushion on the lower surface is vanished by the suction effect on the upper surface, and the overall lift decreases, as shown in Fig. 5.

The pressure distributions along the wing surface at the root and the tip at $\alpha = 0$ are plotted in Fig. 12. For all three cases, there are no

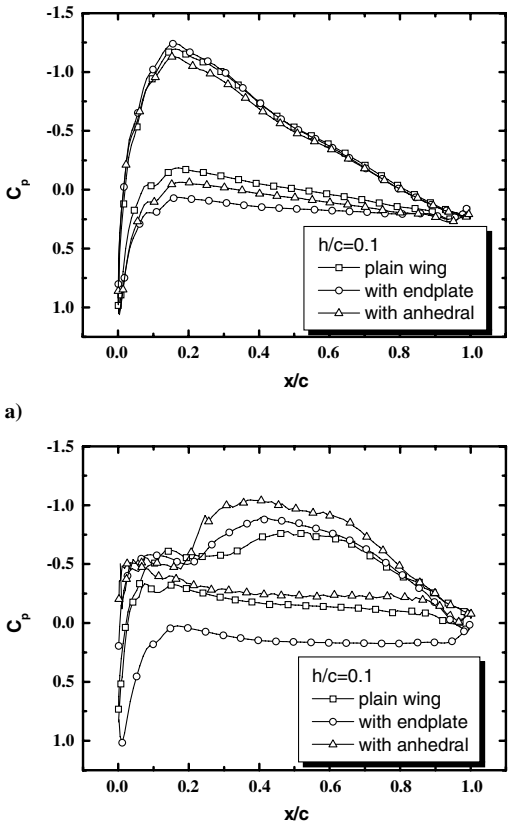

Fig. 11 Comparison of pressure distributions at $\alpha = 0$: a) at midspan and b) at wing tip.

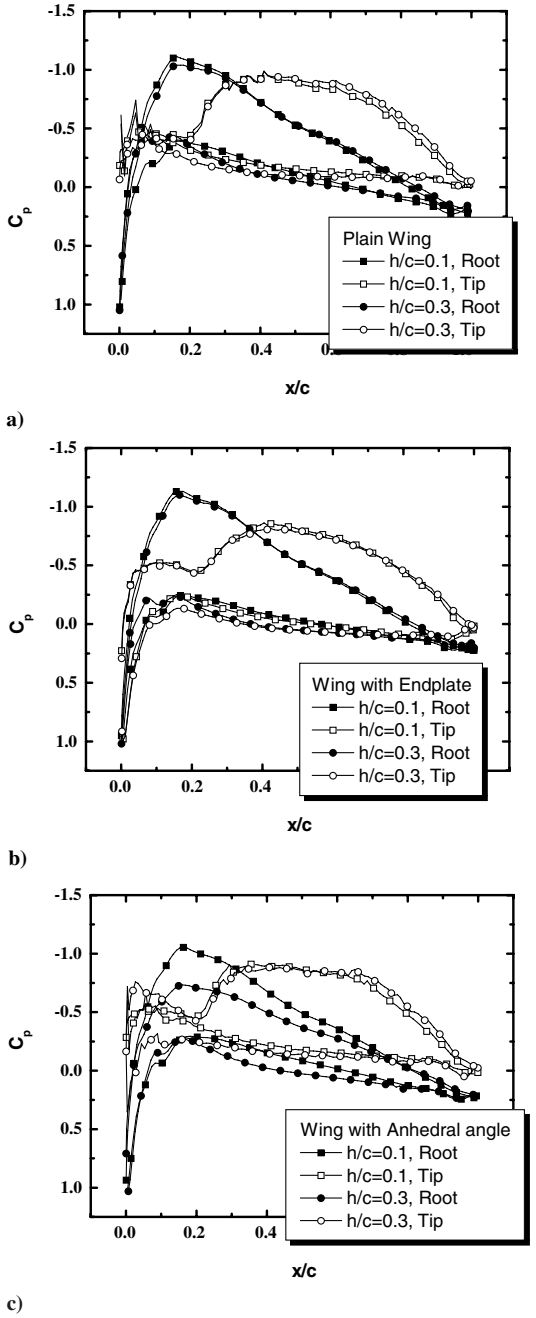

Fig. 12 Pressure distributions on the wing surface at $\alpha = 0$: a) plain wing, b) wing with endplate, and c) wing with anhedral angle.

significant changes in the pressure distributions on the upper wing surface with different heights, except the case with an anhedral angle, which only shows a lower pressure at the wing root because of the skew angle between the symmetric plane and the wing. However, it is clear that the pressure differences on the lower surface are significant and mainly contribute to an increase in lift with a decreasing height, as shown in Fig. 5. Because the normal direction of the lower wing surface at $\alpha = 0$ is almost perpendicular to the flow stream, these increases in lift do not have a strong influence on drag. However, the stagnation point around a leading edge is different because of its favorable direction to the drag: parallel to the air stream. For the wing with an anhedral angle, the stagnation point with ground proximity moves slightly forward, whereas that of the others does not, as shown in Figs. 12a and 12b. As a result, for the case of the anhedral angle, it is expected that the movement of the stagnation point leads to an increase in drag, as shown in Figure 6. On the other hand, an interesting feature in Fig. 12b is that the pressure deviations between the root and the tip are not as significant as found in the others, because the endplate prevents flow from going out through the wing tip. Interestingly, for a WIG effect and small clearances under the tip of the endplates, the nature of the pressures along the wing span may be one dimensional, as Rozhdestvensky [20] pointed out in his study. In Fig. 12b, an improvement in the aerodynamic performance for the case of the endplate is apparently shown. It is interesting to speculate about the reduction of the drag by the ground and the endplate in these results. Figure 12c shows that the stagnation points for a wing with an anhedral angle move upstream with a lower height and result in an increase of the pressure drag, as shown in Fig. 6. The advantage of the induced drag by ground effect cancels out. The designer should be careful in using the anhedral angle to improve the stability of a vehicle.

D. Wing-Tip Vortex

The isosurface and contour of vorticity (x component of vorticity) around the wings are plotted in Figs. 13 and 14, respectively, and visualize their origin and growth of the wing-tip vortices. The negative vorticity in Fig. 14 implies that the center of the rotation is placed along the negative x axis. Two wing-tip vortices, generated at the upper and lower surfaces, flow downstream and grow their radii. The sign of both vortices is the same, and they can be easily merged into one. The two shapes of the wing-tip vortex for the plain wing and a wing with an anhedral angle are similar, whereas that for the endplate is different.

Before the maximum thickness at $x/c = 0.3$, as shown in Fig. 14, the two wing-tip vortices generated at each side have the opposite sign: the upper side (+) and the lower side (−). It is interesting that another vortex is developed on the upper wing surface and the sign of the vortex is negative. Thus, three vortices, two large vortices and one small vortex, are generated for the all cases. After the maximum thickness, the radius of the small vortex rapidly grows along the downstream, because the thickness of the upper wing surface is strongly reduced and splits the next vortex in two at $x/c = 0.5$ and 0.75, as shown in Fig. 14. The strength of the vortex is much stronger than the others and covered at the upper side of the wing tip. On the other hand, the vortex generated on the lower wing surface remains stationary from $x/c = 0.3$ to 1.0 but grows its core radius, as shown in Figs. 14a and 14c. For the plain wing and the wing with an anhedral, the two wing-tip vortices with the negative sign are merged and form a large vortex at $x/c = 1$.

In Fig. 14b, interestingly, the strength of the vorticity for the endplate is much stronger, and the center of the vortex is pushed outward from the wing tip. At the trailing edge, $x/c = 1.0$, the two wing-tip vortices, which are not merged into one, are clearly observed in Figs. 13b and 14b and rapidly diminished along the downstream direction. The plot of the isosurface in Fig. 13b apparently shows the two wing-tip vortices, which are not merged. It can be said that, when the endplate is attached to the WIG effect, a jetlike flow tends to push the wing-tip vortex at the lower surface. The distance between two separated wing-tip vortices is too great to merge at the trailing edge. It is expected that the influence of the wing-tip vortex is considerably reduced.

E. Effect of Reynolds Number

To analyze the effect of the Reynolds numbers on the three wing configurations, computations of various $Re = 0.2 \times 10^6$, 0.49×10^6, and 1.0×10^6, and $h/c = 0.1$, 0.15, 0.2, 0.25, and 0.3 are performed. The only results of C_L and the drag polar at $h/c = 0.1$ are plotted in Figs. 15 and 16, because the other results tend to be similar. Because of the low AR, the influence of the wing-tip vortex reaches the entire wing from tip to root. Different from a two-dimensional or a high-AR wing, the changes of the lift coefficients according to Re are significant. Lift coefficients are increased, but drag coefficients are decreased with Re, as shown in Figs. 15 and 16. The augmentation of the lift coefficient according to the Reynolds numbers is larger at high angles of attack. The case of the wing with an endplate shows the largest augmentation of C_L, but that with the anhedral angle shows the smallest. In contrast, the decrement of C_D for the wing with an anhedral angle is the largest. As a result of an

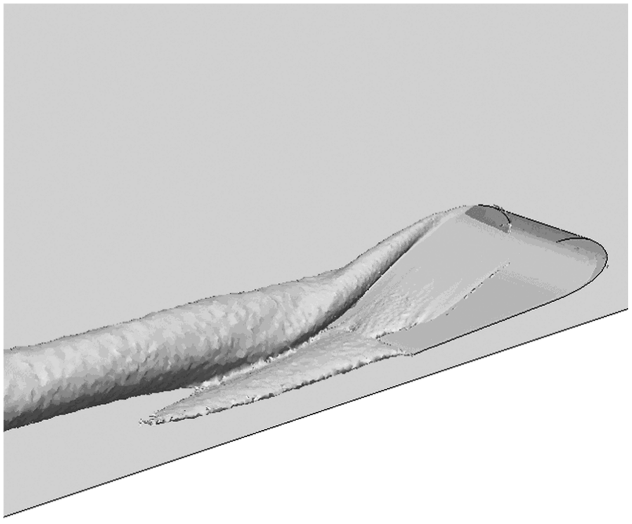

a)

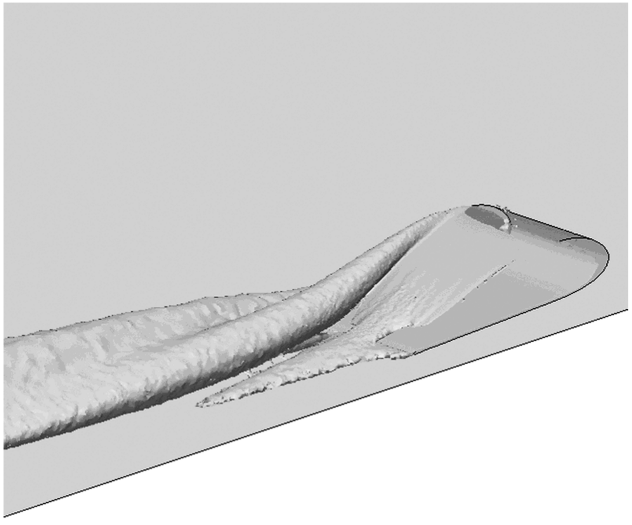

b)

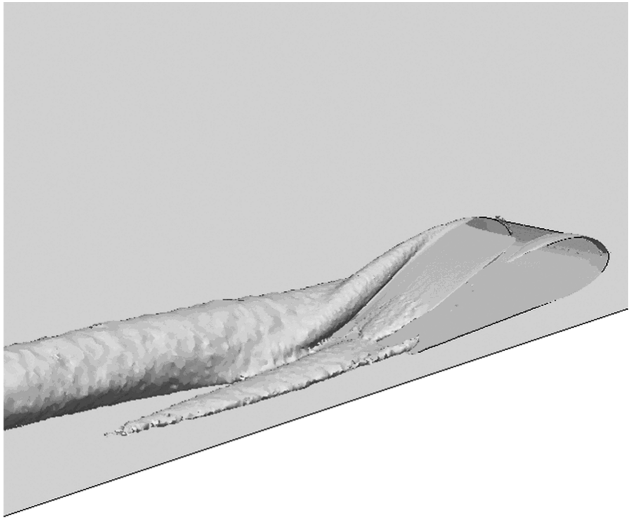

c)

Fig. 13 Effect of wing configuration on vorticity strength: a) isosurface of vorticity strength of plain wing, b) isosurface of vorticity strength of wing with endplate, and c) isosurface of vorticity strength of wing with anhedral angle.

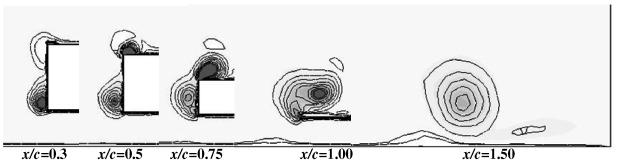

a)

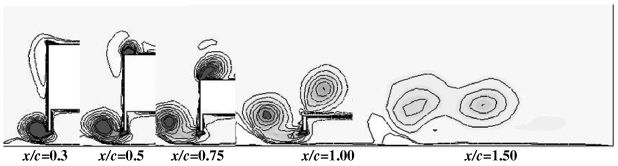

b)

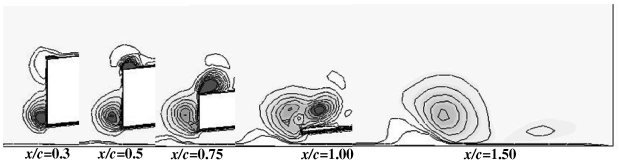

c)

Fig. 14 Vorticity contour from −100 (black) and 20 (white) around wing at $\alpha = 2$ and $h/c = 0.1$: a) plain wing, b) wing with endplate, and c) wing with anhedral angle (line gap is 8).

increase in C_L and a decrease in C_D, L/D is much improved for all the cases. Among the three configurations, the wing with an anhedral angle shows the largest increment in L/D. On the other hand, the largest values of L/D are transferred from $\alpha = 4$ deg to $\alpha = 0$ deg (anhedral angle) and 2 deg (plain and endplate). The gap of the lift coefficients and the drag coefficients between two consecutive

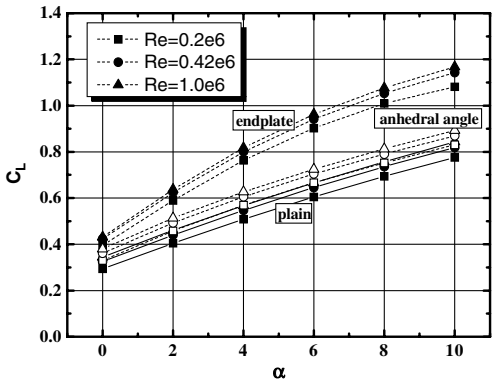

Fig. 15 C_L of three wing configurations with different Reynolds numbers.

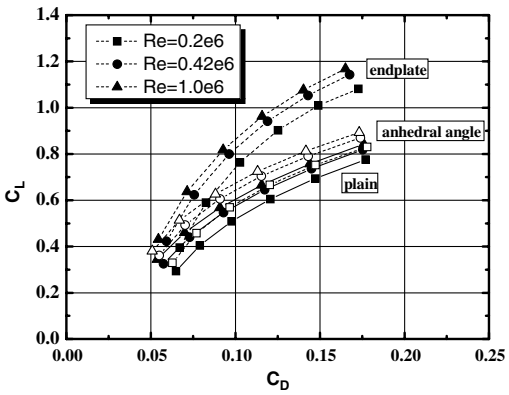

Fig. 16 Drag polars of three wing configurations with different Reynolds numbers.

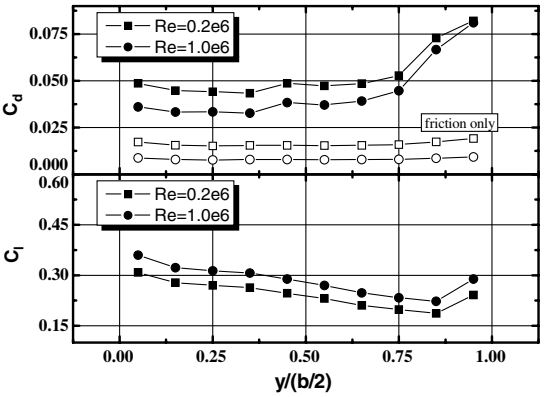

Fig. 17 C_l and C_d along wing span at $h/c = 0.1$ and $\alpha = 0$ deg.

Reynolds numbers, $Re = 0.49 \times 10^6$ and 1.0×10^6, become smaller, as shown in Fig. 16.

To analyze the changes in the lift and the drag with the Reynolds numbers, C_l and C_d are plotted along the wing span in Fig. 17. According to the Reynolds numbers, C_d becomes smaller and the deviation of C_d is stationary along the wing span, except around the wing tip. From the comparison of the deviation of C_d and the fiction drag, the decrease in lift is mainly the result of the friction on the wing surface. However, at the wing tip, C_d suddenly increases as well as the gap of the drag coefficients between two Reynolds numbers becomes smaller because of the wing-tip vortex. In general, the influence of the wing-tip vortex is smaller than that of OGE but still important for the case of a low-aspect-ratio wing.

As shown in Fig. 17, the C_d decreases constantly throughout the wing span. The contribution of friction to the increment in C_l can be ignored. Consequently, the difference of C_l along the wing span between the two Reynolds numbers results from the influence of the wing-tip vortex. Figure 18 shows ω_n at various locations along the chord. For $Re = 1.0 \times 10^6$, the vorticity strength at the core is stronger, as shown in Fig. 18, but the influence of the wing-tip vortex becomes smaller on the wing surface. For the low Reynolds number of $Re = 0.2 \times 10^6$, it is expected that the wing-tip vortex may affect a wide range of the wing surface because of its low moment and high viscosity. It is clear that the influence of the wing-tip vortex becomes wider and stronger along the wing chord. Consequently, the decrement of C_l at $Re = 0.2 \times 10^6$ is mainly the result of the wing-tip vortex.

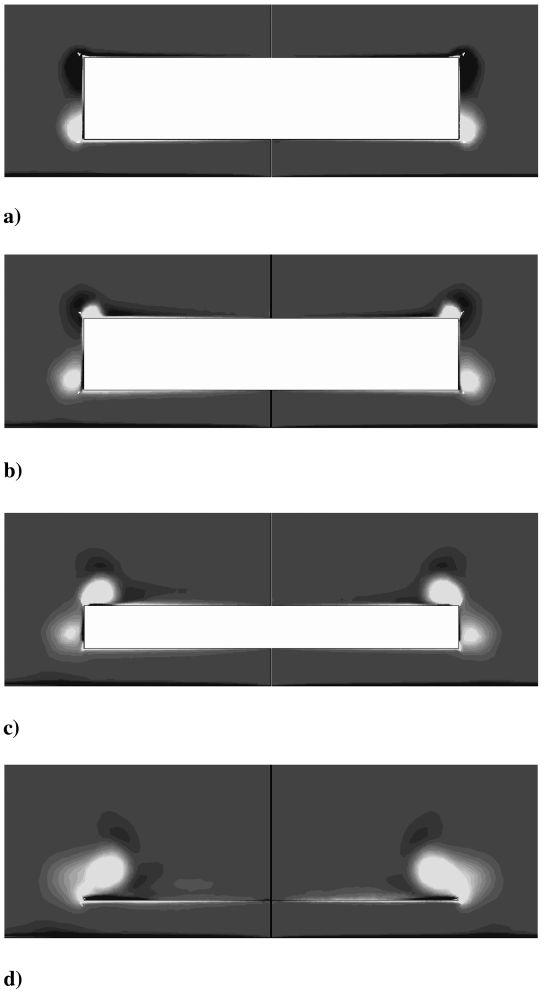

Fig. 18 ω_n contour from −75 (white) to 20 (black) and influence of wing-tip vortex between two Reynolds numbers at $h/c = 0.1$ and $\alpha = 0$ deg; $Re = 0.2 \times 10^6$ (left) and 1.0×10^6 (right): a) $x/c = 0.25$, b) $x/c = 0.5$, c) $x/c = 0.75$, and d) $x/c = 1$.

IV. Conclusions

In this study, a numerical investigation has been conducted to analyze the effect of an endplate and an anhedral angle on the wings IGE. The results from three cases (a plain wing, a wing with an endplate, and a wing with an anhedral angle) show the general ground effect well: that the ground increases the lift as well as decreases the drag with the lower height between the wing and the ground. Among them, the endplate preventing the high-pressure air from escaping out of the lower wing surface augments the lift, whereas the drag remains constant or changes slightly. The endplate can maximize the ground effect and result in a higher lift–drag ratio among the three cases. However, in terms of the static height stability, the endplate is not favorable; the anhedral angle is the best.

Maximum lift–drag ratios for the plain wing without an endplate and an anhedral angle and the wing with an endplate are recorded at $\alpha = 2$ and 4, respectively, because of their low increment of lift at a low α and high increment of drag at a high α. The endplate captures the high-pressure air under the wing and increases the C_L and the L/D further. On the other hand, the wing-tip vortex for the endplate is separated into two and has been diminished rapidly along the downstream. This may be one of the significant reasons for the decrease in the induced drag for the wing with the endplate. However, the plain wing and the wing with an endplate do not satisfy the HS condition at $\alpha = 6 \sim 10$ deg and $\alpha = 4 \sim 10$ deg, respectively. The case of an anhedral angle satisfies the HS condition for all α and h/c and is more favorable for HS. It is found that the stability is mainly affected by the X_h rather than X_α, which slightly decreases as the height is decreased. Briefly, X_α moves upstream, whereas X_h moves downstream at the low α but upstream at the high α. Moving X_h upstream is favorable for the static height stability.

The drag for the wing with an anhedral angle does not decrease as much as that of the plain wing, but it increases with the lower height because of an increase in the pressure drag at the leading edge by a stagnation point moving upstream. The area of the leading edge is small but has a strong effect on drag. For the wing with an anhedral angle, the pressure drag at the leading edge cancels out all the advantages of the drag reduction by ground effect and results in an increase in the drag with a lower height.

Among the three configurations considered in this study, the anhedral angle shows the intermediate L/D as well as a large stability margin, and it has the considerable potential for the WIG effect craft. The combination of an endplate and an anhedral angle is expected to further improve the aerodynamic characteristics and the static height stability IGE. The investigation of the combination wing will be performed in the near future.

References

[1] "Wingship Investigation," Vol. 1, Advanced Research Projects Agency Rept. A979492, Arlington, VA, 1994.

[2] Wieselsberger, C., "Wing Resistance Near the Ground," NACA TM 77, 1922.

[3] Fink, M. P., and Lastinger, J. L., "Aerodynamic Characteristics of Low-Aspect-Ratio Wings in Close Proximity to the Ground," NASA

TN D-926, 1961.
[4] Carter, A. W., "Effect of Ground Proximity on the Aerodynamic Characteristics of Aspect-Ratio-1 Airfoils With and Without End Plate," NASA TN D-970, 1961.
[5] Ahmed, M. R., Takasaki, T., and Kohama, Y., "Aerodynamics of a NACA4412 Airfoil in Ground Effect," *AIAA Journal*, Vol. 45, No. 1, 2007, pp. 37–47. doi:10.2514/1.23872
[6] Joh, C. Y., and Kim, Y. J., "Computational Aerodynamic Analysis of Airfoil for WIG (Wing-In-Ground-Effect) Craft," *Journal of the Korean Society for Aeronautical and Space Sciences*, Vol. 32, No. 8, 2004, pp. 37–46 (in Korean).
[7] Hsiun, C., and Chen, C., "Aerodynamic Characteristics of a Two-Dimensional Airfoil with Ground Effect," *Journal of Aircraft*, Vol. 33, No. 2, 1996, pp. 386–392. doi:10.2514/3.46949
[8] Recant, I. G., "Wing-Tunnel Investigation of Ground Effect on Wing with Flaps," NACA TN 705, 1939.
[9] Park, K. W., and Lee, J. H., "Influence of Endplate on Aerodynamic Characteristics of Low-Aspect-Ratio Wing in Ground Effect," *Journal of Mechanical Science and Technology*, Vol. 22, No. 12, 2008, pp. 2578–2589. doi:10.1007/s12206-008-0805-y
[10] Rodi, W., *Turbulence Models and Their Applications in Hydraulics: a State Art of Review*, International Assoc. for Hydraulic Research, Delft, The Netherlands, 1984.
[11] STAR-CD, Software, Ver. 4, CD-adapco, London, 2006.
[12] Patankar, S. V., *Numerical Heat Transfer and Fluid Flow*, McGraw–Hill, New York, 1980.
[13] Park, K. W., Hong, C. H., Kim, K. S., and Lee, J. H., "Effect of Endplate Shape on Performance and Stability of Wings-in Ground (WIG) Craft," *Proceedings of World Academy of Science, Engineering, and Technology*, Vol. 47, Nov. 2008, pp. 296–302.
[14] Ahmed, M. R., and Sharma, S. D., "An Investigation on the Aerodynamics of a Symmetrical Airfoil in Ground Effect," *Experimental Thermal and Fluid Science*, Vol. 29, No. 6, 2005, pp. 633–647. doi:10.1016/j.expthermflusci.2004.09.001
[15] Ahmed, N. A., and Goonaratne, J., "Lift Augmentation of a Low-Aspect-Ratio Thick Wing in Ground Effect," *Journal of Aircraft*, Vol. 39, No. 2, 2002, pp. 381–384. doi:10.2514/2.2940
[16] Raymond, A. E., "Ground Influence on Airfoils," NACA TM 67, 1921.
[17] Irodov, R. D., "Criteria of Longitudinal Stability of Ekranoplan," *Ucheniye Zapiski TSAGI*, Vol. 1, No. 4, 1970, pp. 63–74.
[18] Lee, J. H., Lee, S. H., and Park, K. W., "Global Shape Optimization of Airfoil Using Multi-Objective Genetic Algorithm," *Transactions of the Korean Society of Mechanical Engineers, A*, Vol. 29, No. 10, 2005, pp. 1163–1171 (In Korean).
[19] Kornev, N., and Matveev, K., "Complex Numerical Modeling of Dynamics and Crashes of Wing-In-Ground Vehicles," 41st Aerospace Sciences Meeting and Exhibit, AIAA Paper 2003-600, Jan. 2003.
[20] Rozhdestvensky, K. V., *Aerodynamics of a Lifting System in Extreme Ground Effect*, Springer–Verlag, Berlin, 2000.